Supporting Information for
Crystal Structure and Stability of Ammonium Azide under High Pressure

Guozhao Zhang[1,2] , Haiwa Zhang[2], Sandra Ninet[2], Hongyang Zhu[3], Cailong Liu[4], Jean-Paul Itié[5], Chunxiao Gao[1,], and Frédéric Datchi[2,*]*

[1]State Key Laboratory of Superhard Materials, Jilin University, Changchun 130012, China.
[2]Institut de Minéralogie, de Physique des Matériaux et de Cosmochimie (IMPMC), Sorbonne Université, CNRS UMR 7590, MNHN, 4 Place Jussieu, F-75005 Paris, France.
[3]School of Physics and Electronic Engineering, Linyi University, Linyi 276005, China
[4]Shandong Key Laboratory of Optical Communication Science and Technology, School of Physical Science and Information Technology of Liaocheng University, Liaocheng 252059, China
[5]Synchrotron Soleil, L'Orme des Merisiers, Saint-Aubin, BP 48, 91192 Gif-sur-Yvette Cedex, France.
*Corresponding Authors e-mail: cc060109@qq.com; frederic.datchi@sorbonne-universite.fr

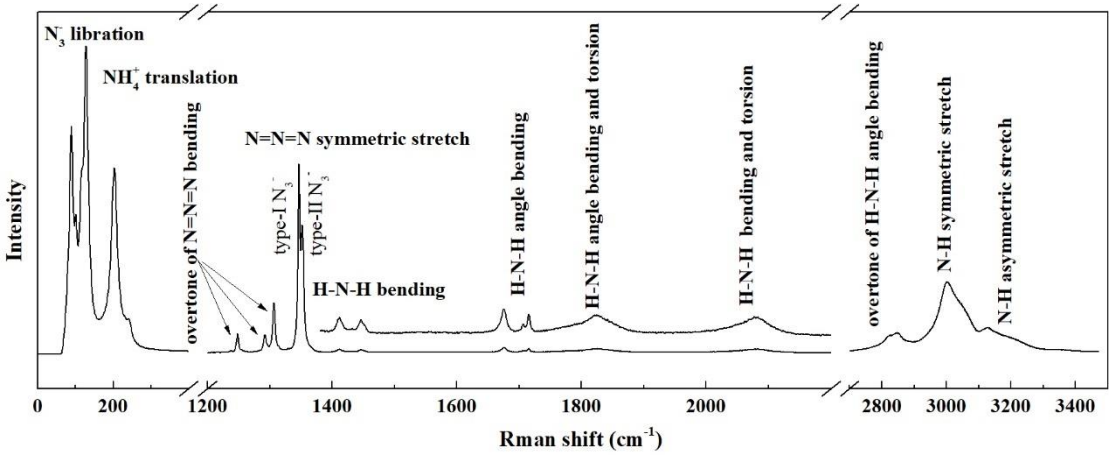

Figure S1. Raman spectra of the synthesized NH_4N_3 powder sample at ambient conditions.

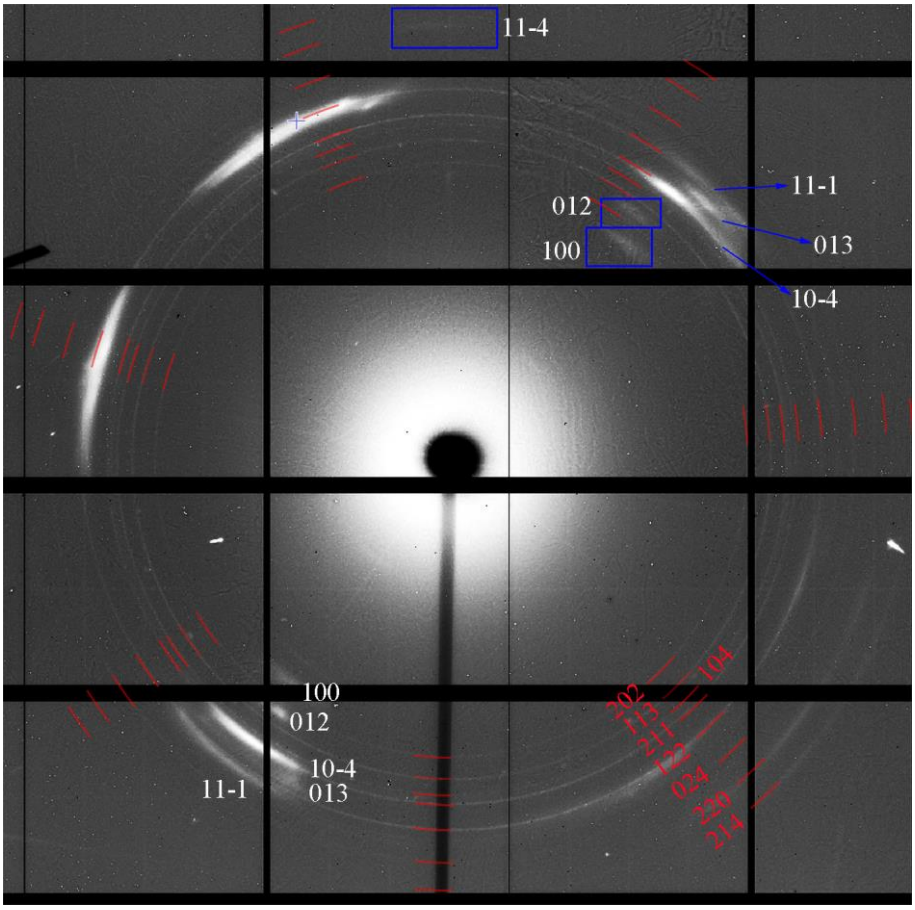

Figure S2. X-ray diffraction image of the AA sample embedded in nitrogen pressure medium at 28.2 GPa – 300 K, showing that this sample is highly textured. The (hkl) indices in white refer to the reflections from the AA-*P2/c* phase. The red dashed circles with red (hkl) indices represent the diffraction rings from the ε phase of nitrogen[1].

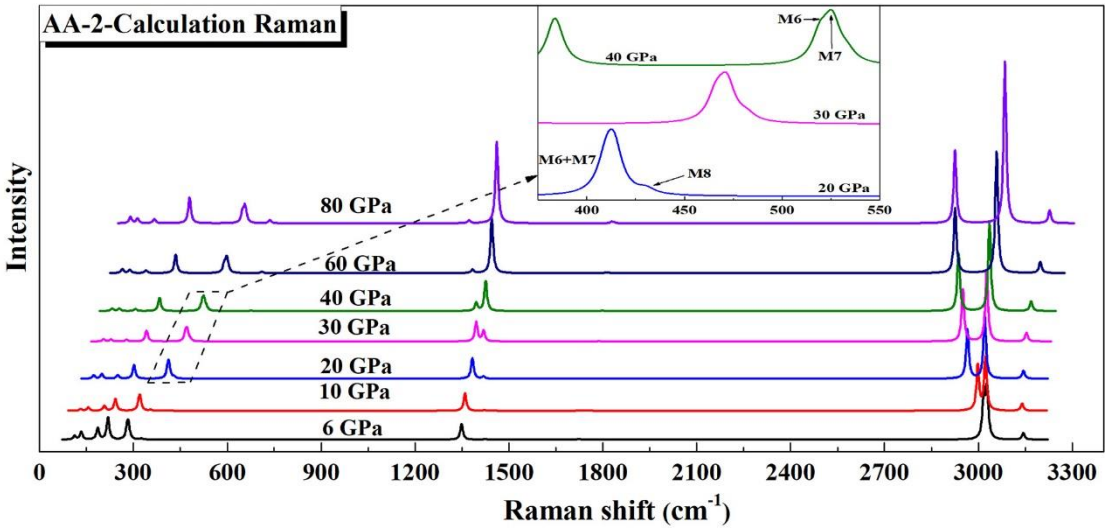

Figure S3. Calculated Raman spectra of AA-*P2/c* at different pressures.

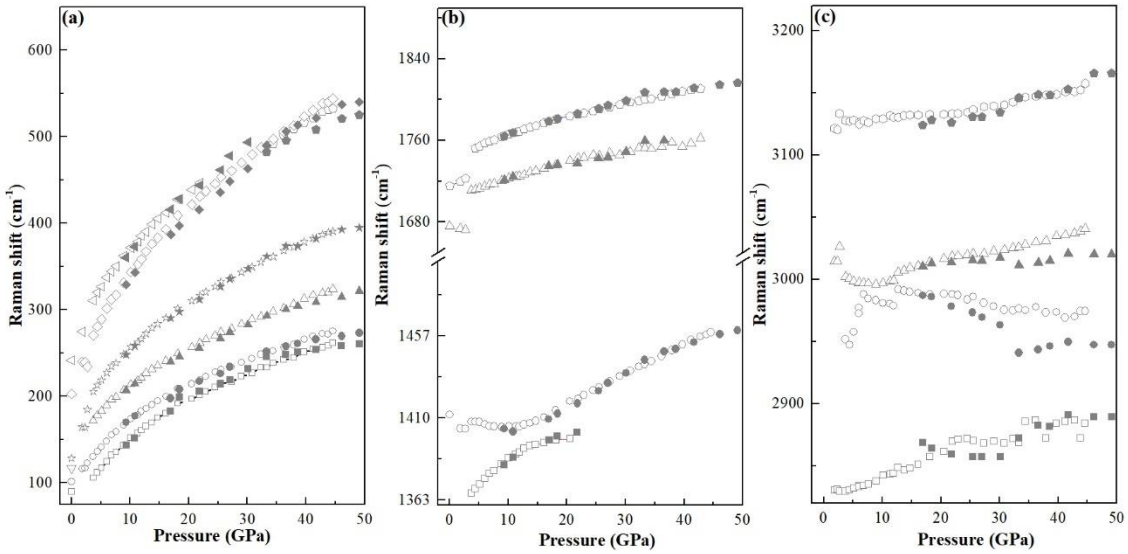

Figure S4. Comparison between the experimental Raman frequencies of AA as a function of pressure, measured with the sample with argon pressure medium (open symbols) and no pressure medium (solid symbols). The difference in frequency measured in the two runs is small for most of the modes, which results from the fact that AA is a soft material and act itself as a good pressure medium. The larger difference observed in the modes near 3000 cm^{-1} comes

from the fact that this band is composed of three modes which are not well resolved, inducing larger uncertainties in the postion of individual components.

Table S1. Comparison of our calculation results for the DFT optimized structures at ambient pressure with previous theoretical calculations.

Phase	Parameter	This work	Other calculations
AA-*Pmna* (Z=4)	a (Å)	9.010	9.094[a], 9.205[b], 8.754[c], 9.015[d]
	b (Å)	3.887	3.904[a], 3.809[b], 3.636[c], 3.809[d]
	c (Å)	8.620	8.627[a], 8.546[b], 8.356[c], 8.551[d]
	V (Å^3)	304.88	306.28[a], 299.6[b], 266.0[c], 293.7[d]
	E_0 (*eV/atom*)	-146.267	-143.512[c], -143.51[d]
AA-*P2/c* (Z=2)	a(Å)	3.669	2.816[e]
	b(Å)	3.665	2.859[e]
	c(Å)	13.481	10.112[e]
	β (°)	123.32	118.08[e]
	V(Å^3)	151.44	71.83[e]
	E_0 (*eV/atom*)	-146.25	
TTZ (*P-1*, Z=4)	a(Å)	10.527	10.575[b], 10.469d
	b(Å)	7.056	6.863[b], 6.888[d]
	c(Å)	4.107	4.026[b], 4.081[d]
	α(°)	103.52	102.60[b], 102.63[d]
	β(°)	88.34	87.463[b], 97.94[d]
	γ(°)	104.54	104.25[b], 104.22[d]
	V(Å^3)	286.96	278.29[d]
	E_0 (*eV/atom*)	-146.12	-143.39[b], -143.39[d]
HNS-1 ($P2_1/m$, Z=2)	a(Å)	8.452	8.185[b], 8.395[d], 8.594[f]
	b(Å)	2.318	2.311[b], 2.312[d], 2.317[f]

	c(*Å*)	3.056	3.064[b], 3.05[d], 3.002[f]
	β(°)	106.08	107.38[b], 107.34[d], 105.74[f]
	V(*Å*^{3})	46.56	55.310[b], 56.53[d], 57.54[f]
	E_0(*eV/atom*)	-145.90	-143.16[b], -143.19[d]
	a(*Å*)	8.480	8.183[d], 8.235[g]
HNS-2	c(*Å*)	4.684	4.211[d], 4.134[g]
(*P4$_2$/n*, Z=4)	V(*Å*^{3})	336.81	281.96[d],
	E_0(*eV/atom*)	-145.89	-143.16[d], -143.19[g]

[a]Ref.[2], [b]Ref[3]., [c]Ref.[4], [d]Ref.[5], [e]Ref.[6], [f]Ref.[7], [g]Ref.[8].

Table S2. Details of the Rietveld refinement of the XRD patterns at different pressures.

Pressure	0.9 GPa	3.0 GPa	7.3 GPa	13.8 GPa
cryst syst	Orthorhombic	Monoclinic	Monoclinic	Monoclinic
space group	*Pmna*	*P2/c*	*P2/c*	*P2/c*
a (Å)	8.843	3.532	3.421	3.213
b (Å)	3.715	3.504	3.420	3.300
c (Å)	8.611	11.586	11.124	10.464
α (deg)	90	90	90	90
β (deg)	90	117.8	116.1	112.0
γ (deg)	90	90	90	90
Volume (Å3)	282.9	126.9	116.8	102.9
R-factors	R_{Bragg}=0.06 R_f=0.076 R_p=0.005 R_{wp}=0.008 R_{exp}=0.030 Chi2=0.07	R_{Bragg}=0.052 R_f=0.105 R_p=0.002 R_{wp}=0.003 R_{exp}=0.029 Chi2=0.01	R_{Bragg}=0.045 R_f=0.077 R_p=0.0024 R_{wp}=0.0037 R_{exp}=0.029 Chi2=0.016	R_{Bragg}=0.015 R_f=0.016 R_p=0.0025 R_{wp}=0.004 R_{exp}=0.029 Chi2=0.02
Radiation	Mo Kα ($\lambda_{K\alpha1}$=0.70926 Å, $\lambda_{K\alpha2}$ = 0.713590 Å)			
2θ range	6.0-38°			
Step	0.011			

Table S3. Experimental P-V dataset for the P2/c phase from the XRD experiments. Run 1 used a sample without pressure medium, Run 2 used nitrogen as pressure medium. Pressure in GPa, Volume in $Å^3$/molecule.

XRD Run	Pressure	Volume	XRD Run	Pressure	Volume
1	0.9(*Pmna*)	17.681	2	32.5	10.704
1	3.0	15.855	2	35.4	10.564
1	7.3	14.603	2	37.3	10.509
1	13.8	12.866	2	38.7	10.436
2	27.3	11.367	2	40.4	10.296
2	28.0	11.104	2	44.7	10.043
2	29.3	10.985			

Table S4. Lattice parameters and volume of the *P2/c* phase as a function of pressure obtained in present theoretical calculations.

Pressure (GPa)	a (*Å*)	b (*Å*)	c (*Å*)	β (°)	V ($Å^3$)
0	3.682	3.678	13.433	122.88	152.77
2	3.532	3.532	12.209	117.77	134.76
4	3.449	3.452	11.735	116.46	125.08
6	3.388	3.389	11.467	115.65	118.70
10	3.298	3.297	11.080	114.56	109.57
12.5	3.252	3.253	10.919	114.09	105.44
20	3.149	3.152	10.611	113.09	96.85
30	3.037	3.045	10.384	111.98	89.05
40	2.949	2.947	10.264	110.95	83.30
50	2.876	2.875	10.187	110.23	79.00
60	2.817	2.816	10.118	109.65	75.58
70	2.763	2.761	10.081	109.12	72.68
80	2.722	2.719	10.019	108.74	70.22
90	2.686	2.682	9.958	108.38	68.07
100	2.6466	2.6455	9.938	108.06	66.16

Table S5. Calculated optical modes of AA-*P2/c* at 6.0 GPa.

Mode	Symmetry	Frequency cm-1	IR	IR Intensity	Raman	Raman Intensity	Assignment
M4	Bg	112.62	N	0.00	Y	3.00	N3 Rot. + NH4 Trans.
M5	Ag	133.50	N	0.00	Y	8.66	N3 Rot. + NH4 Trans.
M6	Bg	280.44	N	0.00	Y	42.56	N3 Rot. + NH4 Trans.
M7	Ag	284.43	N	0.00	Y	48.64	N3 Rot. + NH4 Trans.
M8	Bg	325.46	N	0.00	Y	5.34	N3 Rot. + NH4 Trans.
M9	Bg	186.16	N	0.00	Y	23.11	N3 Rot. + NH4 Trans.
M10	Au	140.20	Y	3.50	N	0.00	Lattice Trans.
M11	Bu	140.66	Y	3.71	N	0.00	Lattice Trans.
M12	Bu	250.06	Y	266.69	N	0.00	Lattice Trans.
M13	Au	251.38	Y	280.31	N	0.00	Lattice Trans.
M14	Bu	273.22	Y	562.22	N	0.00	Lattice Trans.
M15	Ag	218.80	N	0.00	Y	57.34	Lattice Rot.
M16	Au	204.11	Y	3.07	N	0.00	N3 Trans.
M17	Bu	541.82	Y	8.00	N	0.00	NH4 Torsion.
M18	Au	544.79	Y	3.59	N	0.00	NH4 Torsion.
M19	Bg	555.10	N	0.00	Y	0.00	NH4 Torsion.
M20	Ag	556.53	N	0.00	Y	0.20	NH4 Torsion.
M21	Bu	591.55	Y	9.59	N	0.00	NH4 Torsion.
M22	Bg	614.70	N	0.00	Y	0.53	NH4 Torsion.
M23	Bu	617.30	Y	13.79	N	0.00	N3 Bend.
M24	Au	618.22	Y	11.31	N	0.00	N3 Bend.
M25	Au	646.16	Y	29.05	N	0.00	N3 Bend+NH4 Torsion.
M26	Bu	662.68	Y	18.86	N	0.00	N3 Bend+NH4 Torsion.
M27	Bg	1347.88	N	0.00	Y	14.16	N=N=N Symm str.
M28	Ag	1348.76	N	0.00	Y	479.78	N=N=N Symm str.
M29	Bu	1422.72	Y	313.49	N	0.00	N-H Wagg. + Rock.
M30	Au	1423.80	Y	271.67	N	0.00	N-H Wagg. + Rock.
M31	Bu	1425.94	Y	363.22	N	0.00	N-H Wagg. + Rock.
M32	Bg	1423.84	N	0.00	Y	3.98	N-H Scissor. + Wagg.
M33	Ag	1424.49	N	0.00	Y	12.80	N-H Scissor. + Wagg.
M34	Bg	1439.12	N	0.00	Y	3.31	N-H Scissor. + Wagg.
M35	Au	1720.20	Y	11.23	N	0.00	N-H Bend.
M36	Ag	1724.00	N	0.00	Y	27.50	N-H Bend.
M37	Ag	1752.40	N	0.00	Y	5.33	N-H Bend.
M38	Au	1744.99	Y	2.37	N	0.00	N-H Scissor. + Bend.
M39	Bu	2072.51	Y	4960.00	N	0.00	N=N=N Asymm. str.
M40	Au	2173.24	Y	211.38	N	0.00	N=N=N Asymm. str.

M41	Bu	3011.03	Y	3220.00	N	0.00	N-H Asymm. Str.
M42	Bu	3022.85	Y	5890.00	N	0.00	N-H Asymm. Str.
M43	Au	3013.03	Y	2760.00	N	0.00	N-H Symm. Str.
M44	Ag	3016.87	N	0.00	Y	2300.00	N-H Symm. Str.
M45	Bg	3017.39	N	0.00	Y	2290.00	N-H ASymm. Str.
M46	Au	3023.12	Y	232.23	N	0.00	N-H Symm. Str.
M47	Ag	3027.71	N	0.00	Y	5148.64	N-H Symm. Str.
M48	Bg	3143.54	N	0.00	Y	735.46	N-H ASymm. Str.

REFERENCE

(1) Mills, R.; Olinger, B.; Cromer, D., Structures and Phase Diagrams of N_2 and CO to 13 GPa by X-Ray Diffraction. *J. Chem. Phys.* **1986**, *84*, 2837-2845.

(2) Yedukondalu, N.; Ghule, V. D.; Vaitheeswaran, G., Computational Study of Structural, Electronic, and Optical Properties of Crystalline NH_4N_3. *J. Phys. Chem. C* **2012**, *116*, 16910-16917.

(3) Liu, Q.-J.; Zhang, N.-C.; Wu, J.; Sun, Y.-Y.; Zhang, M.-J.; Liu, F.-S.; Wang, H.-Y.; Liu, Z.-T., Theoretical Insight into the Structural, Elastic and Electronic Properties of N_4H_4 Compounds. *Comput. Mater. Sci.* **2014**, *81*, 582-586.

(4) Liu, Q.-J.; Zeng, W.; Liu, F.-S.; Liu, Z.-T., First-Principles Study of Hydronitrogen Compounds: Molecular Crystalline NH_4N_3 and $N_2H_5N_3$. *Comput. Theor. Chem.* **2013**, *1014*, 37-42.

(5) Yedukondalu, N.; Vaitheeswaran, G.; Anees, P.; Valsakumar, M. C., Phase Stability and Lattice Dynamics of Ammonium Azide under Hydrostatic Compression. *Phys. Chem. Chem. Phys.* **2015**, *17*, 29210-29225.

(6) Yu, H.; Duan, D.; Tian, F.; Liu, H.; Li, D.; Huang, X.; Liu, Y.; Liu, B.; Cui, T., Polymerization of Nitrogen in Ammonium Azide at High Pressures. *J. Phys. Chem. C* **2015**, *119*, 25268-25272.

(7) Hu, A.; Zhang, F., A Hydronitrogen Solid: High Pressure Ab Initio Evolutionary Structure Searches. *J. Phys. Condens. Matter* **2010**, *23*, 022203.

(8) Liu, Q.-J.; Zhang, N.-C.; Sun, Y.-Y.; Zhang, M.-J.; Liu, F.-S.; Liu, Z.-T., Density-Functional Theory Study of the Pressure-Induced Phase Transition in Hydronitrogen Compound N_4H_4. *Phys. Lett. A* **2014**, *378*, 1333-1335.